Journal of Medical Genetics and Clinical Biology
Homepage : https://journal.antispublisher.id/index.php/JMGCB
Email : admin@antispublisher.com

e-ISSN : 3032-1085
JMGCB, Vol. 2, No. 5, May 2025
Page 201-221

Enhancing Antifungal Property and Cytotoxicity profile of Gold Nanoparticles Biosynthesis via Some Filamentous Fungi with in *Silico* Study

Suaded A. Majeed[1], Iman A. J. Al-Timimi[2], Abdullah H. Al-Saadoon[3]
[1,2,3]University of Basrah, Iraq

Check for updates OPEN ACCESS

DOI : https://doi.org/10.61796/jmgcb.v2i5.1312

Sections Info

Article history:
Submitted: March 30, 2025
Final Revised: April 14, 2025
Accepted: April 28, 2025
Published: May 25, 2025

Keywords:
Antifungal
Cytotoxicity
In silico
Filamentous fungi

ABSTRACT

Objective: *To synthesize gold nanoparticles by fungi and testing their susceptibility as antifungals and comparing them with computerized study.* ***Method:*** *Synthesis of gold nanoparticles by some filamentous fungi (Aspergillus, Penicillium and Trichoderma), Au NPs characterised using (Transmission electron microscopy (TEM), Uv-vis spectrophotometer, Fourier transform infrared spectroscopy (FTIR), Energy-dispersive X-ray spectroscopy analyses (EDX), testing them as antifungals against pathogenic fungi (Candida albicans, C. tropicalis, Aspergillus niger, and A. flavus) and compared their results with nystatin as standard antifungal, the study was drawing a with In Silico study.* ***Results:*** *Aspergillus growth rate was more susceptible to nanoparticles, the percentage of growth rate was less than 70% after 48h, while Candida species were not affected by nanoparticles whether Au, and the percentage of growth rate was over 95%. The formation Au NPs confirm using UV-Vis with surface plasmon resonance at 540 nm and TEM images confirm spherical shape with average size 30 nm. The obtained data have been reported that therapeutic doses of nystatin that ranged from 8-1 µg/mL were not toxic significantly, and Au at 25% was not toxic effect significantly on cells growth. In silico study the results showed a characteristic binding affinity and conformational stability of Au-protein combination.* ***Novelty:*** *Synthesis of gold nanoparticles using filamentous fungi is best method and nanoparticles have a moderate antifungal activity compared to standard antifungal drug (nystatin).*

INTRODUCTION

The term nanoscience refers to the studying and investigation of systems that are extremely small size. This modern science represents a great combination among several sciences like chemistry, physics, material science, and biology [1]. Nanoscience deals with the structures and molecules on the scale of nanometres extending from 1 to100 nm [2]. Nanotechnology has gained a huge attention over time [3]. Nanoparticles (NPs) have been emerged as promising products of nanotechnology. NPs are an extensive class of materials that involved within nanoscale size, which include particulate substances that have exceptional features which are useful in many implementations [4,5]. The unique properties of NPs are mostly due to physical features includes optical, penetration of light, absorption and reflection capabilities [6]. The chemical properties as the reactivity of the NPs with the target, stability and sensitivity to factors such as moisture, atmosphere, heat and light determine its applications. Corrosive, anti-corrosive, oxidation, reduction and flammability characteristics of the NPs determine their respective usage [6]. The biological characteristics like antibacterial, anti-fungal, antiviral,

and cytotoxicity properties of the NPs are ideal for biomedical and environmental applications [7]. The NPs are broadly classified into several categories depending on their morphology, size and chemical properties.

Metal Inorganic nanoparticles (MINPs) that are manufactured from metals to nano sizes either by negative or construction methods [8]. Physical and chemical methods are gradually being replaced by green synthesis methods because of issues related to consumption of large amount of energy release of toxic and harmful chemicals, and use of complex equipment and synthesis conditions [9]. In contrast, green synthesis utilizes natural and eco-friendly materials (e.g., reducing agents). Some green materials can also be used as capping agents which not only reduces energy consuming, but also avoids use of toxic and harmful reagents. At present, green synthesis mainly uses microorganisms like fungi [10], bacteria, and algae or extracts from leaves, flowers [11] roots, peelings, fruits, and seeds of various plants [12,13]. Fungi are used in synthesis of metal NPs due to their high ability in tolerance and accumulation of the metals. Fungi are characterized by their ease of growth and synthesis of NPs, due to the ease of handling biomass [14]. The gold nanoparticles exhibit excellent antifungal activity and greater biocidal action [15]. Since antifungal resistance is a critical problem, it was necessary to find new compounds as antifungals, especially those produced by fungi, and therefore fungi were used in the biosynthesis of gold nanoparticles and used as antifungals [16]. Over the past decade, the use of computerized models to predict the results of biological studies has become obvious [17]. This concept is known as *In silico* biology. This concept ultimately helps to better understand and predict chronic human disease, and ultimately facilitates the design of better and more rational approaches to the development and analysis of new drug candidates [18].

In general, rational drug design (RDD) is "the ingenious process of discovering new molecules based on knowledge of the biological target". In the traditional approach, drugs were discovered through trial-and-error methodologies, making the research and development process more time-consuming and expensive. Computational drug design helps scientists understand drug receptor interactions, and also helps reduce time and cost [19]. Molecular docking is a technique that assumes “the preferred direction of one molecule to another molecule when it binds to each other to form a stable compound in three-dimensional spaces". The results of docking are very useful in finding effective drugs against certain diseases [20]. Molecular Dynamic simulation studies (MD) can be used to study the dynamic properties of a system in full atomic detail. Thus, molecular dynamics simulations can be used "to better understand the interactions between proteins, between ligand and protein, so as to predict how proteins or some of their elements bind to each other to achieve the lowest free energy configuration" [21].

This study aims to synthesize gold nanoparticles by fungi which characterized and test their effectiveness as antifungal against filamentous and yeasts pathogenic fungi and compare the results with *in silico* study to offer an effective and sustainable alternative applications as in medicine and biology.

RESEARCH METHOD

Biosynthesis of nanoparticles

Three fungal isolates (*Aspergillus cejpii, Penicillium camemberti* and *Trichoderma asperellum*) were used in the synthesis of gold nanoparticles.

Fungal biomass for preparation

After activation of the fungus on the PDA, a disc of 8mm of the fungal isolates was transferred to 500 ml Erlenmeyer flask containing 250 ml of liquid growth medium (YPGM) broth. Culture incubated at 25 ℃ for seven days, after incubation period the fungal biomass was separated from the culture broth by filtration using Whatman No.1 filter paper. The biomass was washed three times with distilled water to remove any medium components, 10 g of biomass was transferred to 250 mL Erlenmeyer flask contain 100 mL of aqueous solution of the metal (Tetra-Chloroauric acid trihydrate $HAuCl_4.3H_2O$), (Sodium selenite Na_2SeO_3) and the both (0.001-0.003) M of final concentration. The culture was incubated at 25 ℃ for three days, with control (without metal ions), the entire process carried out in complete darkness [22].

Characterization of nanoparticles

The nanoparticles were characterized using UV-vis spectroscopy, FTIR-spectrometer, EDX analysis, and TEM.

The antifungal susceptibility tests

The antifungal susceptibility test against planktonic cells growth Four pathogenic fungal isolates were used in this test, including two yeasts isolates: *Candida albicans* and *C. tropicalis* which isolated from nail infections (onychomycosis) and two filamentous pathogenic fungi: *Aspergillus niger* and *A. flavus* which isolated from ear infections (otomycosis). The antifungal drug Nystatin was used as standard in this test, which compared with (Nystatin+ NPs) and NPs alone to determine the minimum inhibitory concentration (MIC) as well as the minimum fungicidal concentration (MFC). The stock solution of Nystatin was prepared by dissolving 0.0064 g in 100 µL of DMSO (dimethyl sulfoxide), then the volume was completed to 10 mL using sterile SD broth medium to get a final concentration of 64 µ/mL, then took 5 mL of it and completed to 10 mL to get the concentration of 32 µ/mL and this serial dilution was continued until reach to concentration of 0.06 µ/mL. The inoculum size has been adjusted for all fungal isolates according to McFarland scale to a 0.5 McFarland turbidity standard using UV spectrophotometer at 530 nm. Inoculum size was $1.5\text{-}5x10^6$ CFU/mL for *Candida* species, and $2\text{-}3x10^4$ CFU/mL for *Aspergillus* species [23]. These concentrations have been used as standard inoculum in all following experiments. One hundred µL of serial dilutions of antifungal drug was loaded into 96 well microtiter plate. Subsequently, 100 µL of active standard fungal inoculum was added to each well. The set of controls were added to the plate including positive control of 200 µL of an active fungal inoculum only, and another positive one contained 100 µL an active of fungal suspension mixed with 100 µL of SD broth containing the same concentration of an organic solvent DMSO which was used to dissolve the Nystatin initially, a negative control was SD broth medium only. The

absorbance of liquid in each well was quantified at 590 nm using a SkanIt Software for Microplate Readers.

Toxicity

The cell lines used in this experiment is Vero cells Vero cells: are derived from the kidney of an African green monkey, and are one of the more commonly used mammalian continuous cell lines in microbiology, molecular and cell biology research.

Cell viability MTT Assay

Cell viability was determined by MTT assay [24]. Briefly, Vero cells were cultured in DMEM/F12 supplemented with 10% fetal bovine serum and 1% penicillin/ streptomycin. Cells were grown at 37℃ and 5% CO_2 and subcultured at 80-90% confluency. The culture medium was removed from flask containing confluent cells, then, the surface of the adherent cells was rinsed with sterile PBS before applying trypsin-EDTA for cell monolayer detachment. Vero cells were cultured in sterile polystyrene 96-well plates at concentration of $2.5x10^4$ cell /well and incubated at 37℃ and 5% CO_2 for 24 hrs. until the cell confluence reaches to 90% approximately. Then, the medium was discarded, and replaced with100 µL fresh medium containing a different concentrations prepared individually for nanparticles (Au, Se, and hybrid) 25, 50, 75, 100 µg/mL and 1-32 µg/mL for Nystatin and for (Nystatin+ Au NPs) 25:75, 50:50, 75:25 µg/mL, controls tested were the positive control (70% ethanol) for total kill and negative control (only medium). After 48 hrs. the cells were incubated with MTT and incubated for 2-4 hrs. at 37℃ and 5% CO_2. The absorbance was recorded at 570 nm using a SkanIt Software for Microplate Readers, three replicates were performed for each concentration. After subtraction of absorbance values of the blank wells (medium only) from the other absorbance values, percentage cell viability was calculated relative to untreated control wells. The percentage of cell viability was measured by using the equation:

Cell viability% = (mean absorbance of treated cells/mean absorbance of control cells) x 100%

In silico study

Protein Preparation

The crystal structures of *Aspergillus* thioredoxin reductase (PDB ID: 5FRB) and the metalloprotein *Candida albicans* (PDB ID: 5V5Z) were retrieved from the RCSB Protein Data Bank (PDB; https://www.rcsb.org) [25]. For 5FRB, non-essential cofactors, including NADPH and crystallographic water molecules, were removed using Auto Dock Tools 1.5.7 [26]. Polar hydrogens and Kollman united atom charges were added to optimize the protein's electrostatic properties for molecular docking. The selenocysteine residue (UniProt ID: P0A884) in the active site, critical for selenium coordination, was retained to preserve the native metal-binding environment. For 5V5Z, pre-processing involved the removal of non-essential ions and water molecules, followed by the addition of Gasteiger charges to residues ARG76, GLU73, and ASP502, identified as key metal-coordinating residues through structural homology analysis. Both proteins were saved in PDBQT format for subsequent docking simulations.

Ligand Preparation

The ligand Nystatin (PubChem CID: 11953884) was sourced from the PubChem database (https://pubchem.ncbi.nlm.nih.gov) [27] and modified with gold (Au) to evaluate metal-dependent binding mechanisms. The base structure of Nystatin was drawn and optimized using Chem Draw 20.0 (PerkinElmer, Inc.; https://perkinelmer.com/products/chemdraw), with metal ions manually incorporated into its scaffold using coordination geometries derived from green synthesis methodologies [28] (Figure 1). Energy minimization was performed using the MMFF94 force field to ensure structural stability [19]. Ligands were converted to three-dimensional PDBQT format using Open Babel 3.1.1 (https://openbabel.org) with the command: Bash " obabel -i sdf nystatin_metal.sdf -o pdbqt -O nystatin_metal.pdbqt --gen3d "Partial atomic charges were assigned via the Gasteiger method and metal-specific parameters, including van der Waals radii and coordination bonds, were defined using AutoDock's metal-binding force field [26].

Virtual Screening and Molecular Docking

Initial virtual screening was conducted using PyRx 0.8 (https://pyrx.sourceforge.io) integrated with Auto Dock Vina https://vina.scripps.edu). For 5FRB, a grid box of 25 × 25 × 25 Å (spacing: 1.0 Å) was centred on catalytic residues ASP493, THR498, and TYR500 to target the selenium-binding pocket. The exhaustiveness parameter was set to 12 to balance computational efficiency and conformational diversity, with the top 10 ligand poses retained for refinement.

Refined docking was performed using Auto Dock 4.2.6 (https://autodock.scripps.edu) with the Lamarckian Genetic Algorithm (LGA). Parameters included 100 independent runs per ligand, a population size of 150, 2.5 million energy evaluations, and mutation/crossover rates of 0.02/0.8. For 5FRB, the grid box (40 × 40 × 40 points) was centered on the catalytic residues ASP493, THR498, and TYR500 to prioritize gold (Au) coordination. Metal coordination geometries were prioritized during conformational sampling, and final binding poses were selected based on clustering analysis and binding energy (ΔG). Both proteins underwent identical parameterization to ensure methodological consistency, with specific grid adjustments reflecting their distinct active site architectures.

Interaction Analysis

Protein-ligand interactions, including hydrogen bonds, hydrophobic contacts, and van der Waals forces, were analyzed using PLIP (Protein-Ligand Interaction Profiler; https://plip-tool.biotec.tu-dresden.de) [29]. Binding energies and root-mean-square deviation (RMSD) values were extracted from AutoDock output files. Solvent-accessible surface area (SASA) calculations for binding site residues, such as ARG76 (35.75 Å²) and GLU73 (35.86 Å²) in 5V5Z, were performed using PyMOL 2.5 (https://pymol.org) to quantify flexibility.

RESULTS AND DISCUSSION

Results

Biosynthesis of Au NPs

Au NPs was synthesized by using the three fungal isolates *(A. cejpii, P. camemberti, and T. asperellum)*, The synthesis of Au NPs is recognized by the colour change of the mixture of biomass and $HAuCl_4.3H_2O$ (0.001M) aqueous solution from yellow to ruby colour. In comparison with the control flask, the change in the colour of biomass mixture after 72h at a temperature of 25°C can be observed in Figure 1.

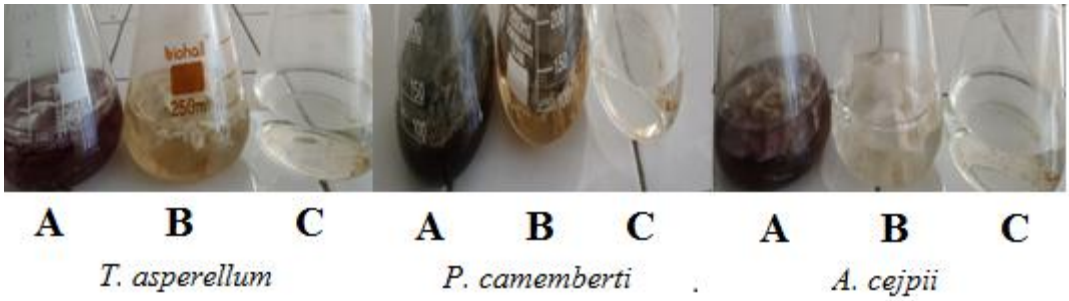

Figure 1. The change in colour of gold aqueous solution after 72h. A- Fungal biomass with Au aqueous solution, B-Fungal biomass with medium, C-Au aqueous solution.

The experiment showed that the Au NPs began to withdraw into the fungus after a period of more than three days Figure 2.

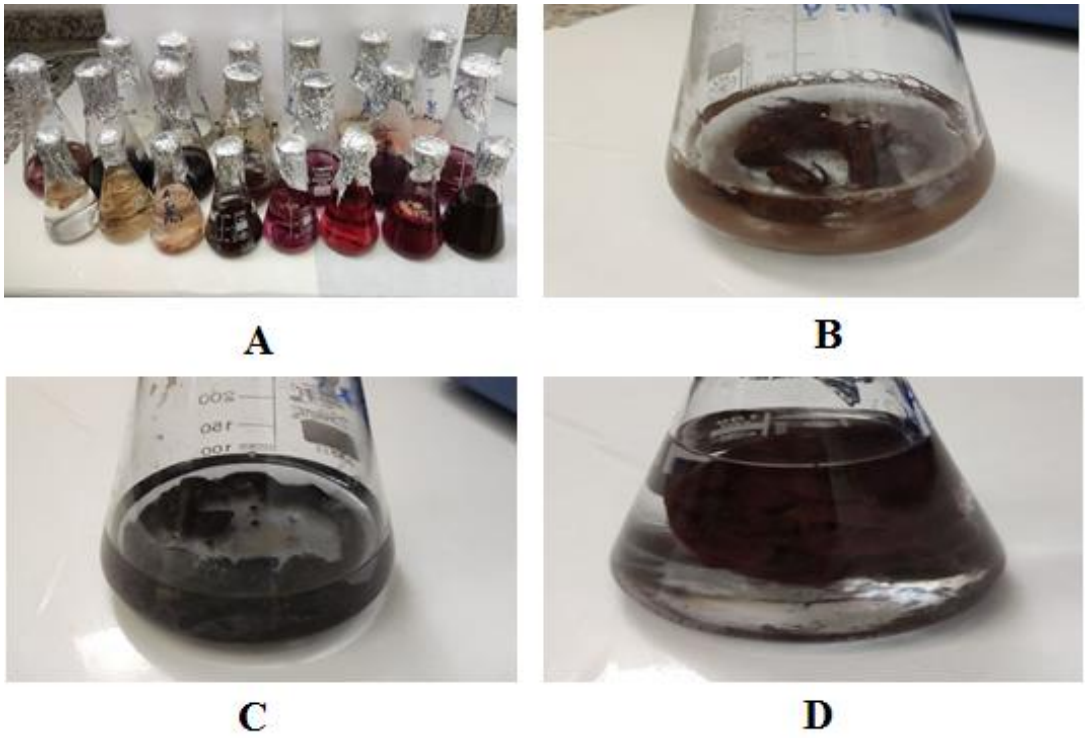

Figure 2. The withdrawal of Au NPs inside the fungal isolates after more than three days, A-before three days, B-*T. asperellum* (after 72h), C-*P. camemberti* (after 72h), D-*A. cejpii* (after three days).

Characterization of metal nanoparticles

UV-Vis spectroscopy

The UV–vis spectrometry is used to confirm the production of Au NPs. In this analysis, the absorption of the ultraviolet ray at different wavelengths is considered. Since Au has an absorption spectrum in the range of 500–600 nm. The important evidence suggesting the formation of Au NPs is the maximum absorption peak at 540 nm [30], see Figure 3.

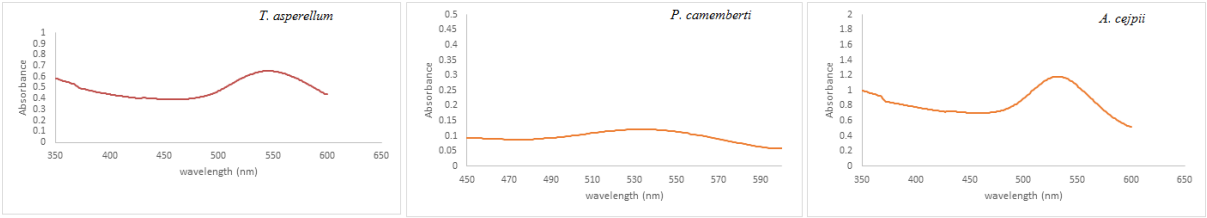

Figure 3. The UV–Vis spectrometry analysis for the Au NPs by fungi.

FTIR analysis

FTIR technic can provide chemical characterization via identifiable spectral features. The vibrational spectra of fungus biomolecules as control and NPs/fungus can be used for simple and rapid identification through straightforward correlation between spectra and biochemical composition. Evidently FTIR has more potential for general studies of such bio particles; biochemical analysis of fungus by FTIR could provide economical, reliable, simple and timely information [31]. Formation of Au NPs by the three fungal isolate and the interaction between the synthesized NPs and active metabolites of the three fungal isolates were further investigated by FTIR-spectroscopic analyses. FTIR spectra of culture of the three isolates (black line) as well as the NPs (red line) were recorded (in the range 400–4000 cm^{-1}). Important FTIR regions for fungus: Broad peak at 3269 cm^{-1} relates to O-H and N-H stretching (st.). Two peaks at 2922-2859 cm^{-1} refer to C-H stretching (st.). Absorption at 1700-1500 cm^{-1} related to chitin and proteins compound in the cell wall; the two peaks at 1741 and 1369 cm^{-1} can be attributed to free fatty acids (C=O stretch in carboxylic acids and C–O–H bending, respectively); in addition, it has strong peaks at 1629 and 1026 cm^{-1} that can be attributed to phospholipids (C=O stretch in esters and P–O– stretch, respectively). Absorption at 1200-900 cm^{-1} may refers to carbohydrate bands C-O-C. The appearance of the C≡N stretching peak, ranging around 2300 cm^{-1}, in nitrile compounds. Figure 4 confirmed that the disappearance and shifted of several bands for the infrared Au NPs/fungus spectrum which could be comfirmed using as reducing agent.

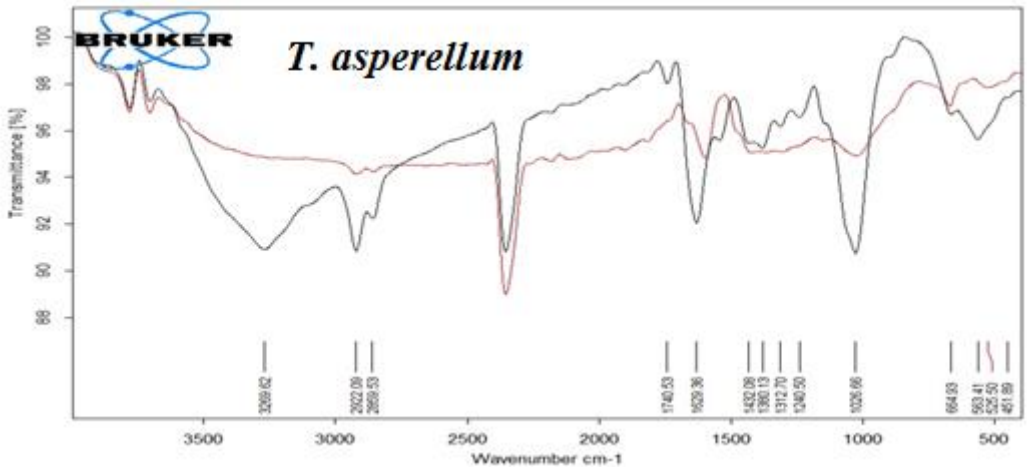

Figure 4. FTIR spectra of the fungal culture (Black line) and the synthesized AuNPs (Red line).

Energy-dispersive X-ray spectroscopy (EDX)

Energy-dispersive X-ray spectroscopy (EDX) is one analytical method used for the structural analysis of samples. According to the provided EDX diagram, the presence of oxygen (O), chloride (Cl), and confirm present gold (Au) atoms in the synthesized sample Au NPs as shown in Figure 5.

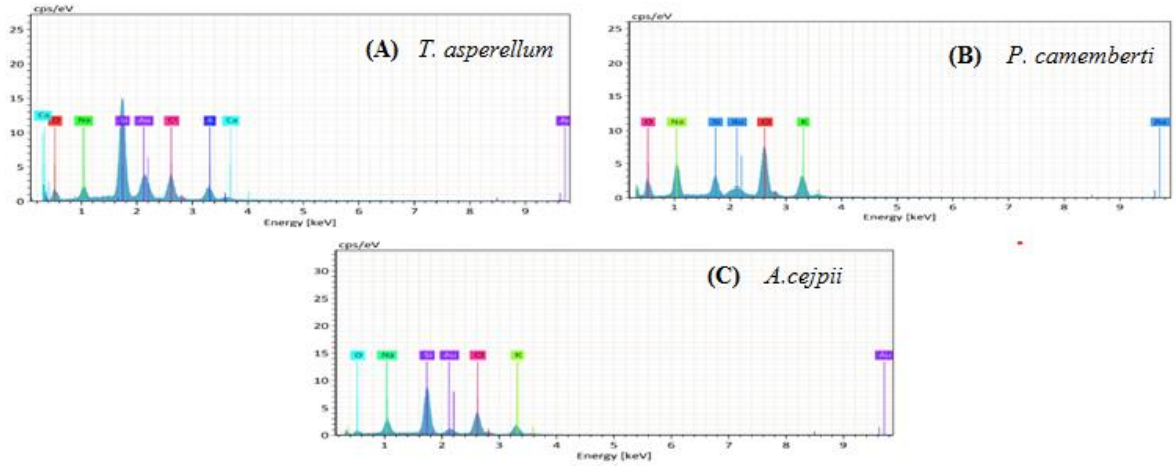

Figure 5. The EDX diagram of Au NPs (A, B and C)

Transmission electron microscopy (TEM)

The TEM results of *T. asperellum* revealed the Au NPs inside the fungal cell. According to the pictures the shape of Au NPs spherical and abundant inside the fungal cell, see Figure 6.

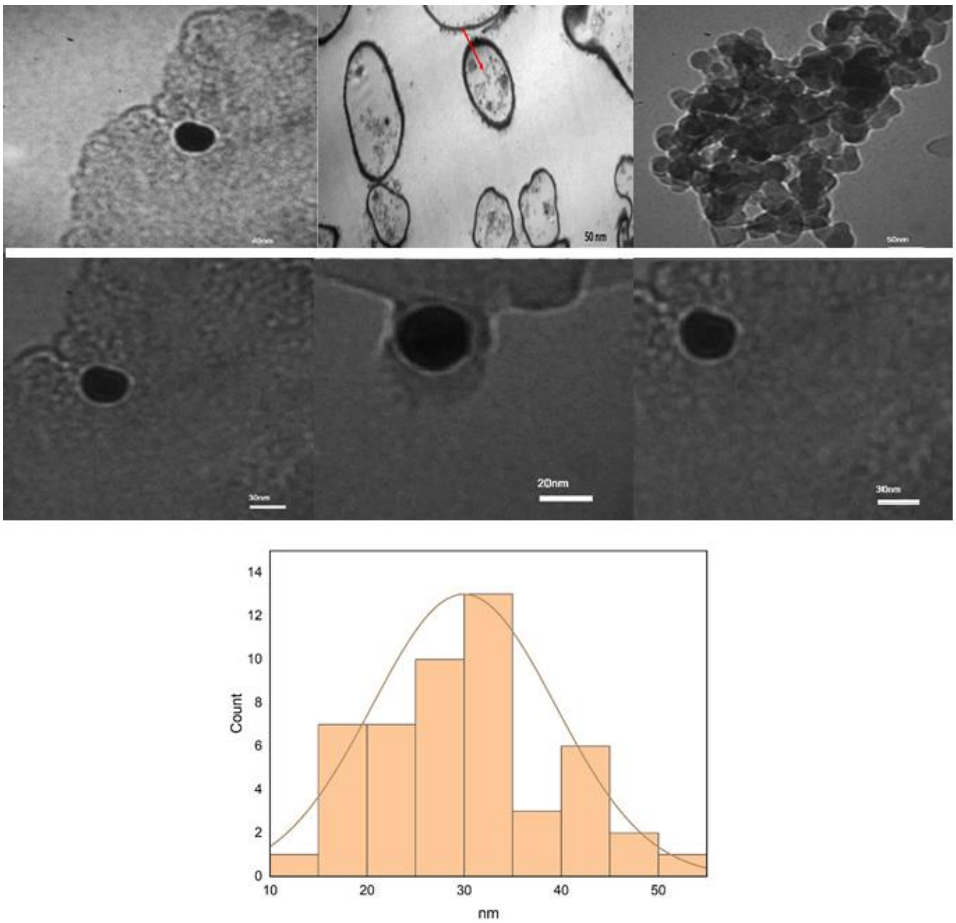

Figure 6. Represent the TEM images of spherical Au NPs with size average 30 nm.

The antifungal susceptibility tests

Antifungal susceptibility testing was performed using Nystatin against planktonic cells (96-well plates). The MIC and MFC for Nystatin are presented in Table 1, Figure 7, 8, 9 and 10. The higher value of MIC was for *A. flavus* (2), followed by *C. albicans* and *C. tropicalis* [1], while the less value for *A. niger* (0.5).

Table 1. The MIC and MFC of Nystatin against four tested fungal isolates.

Antimicrobial agent	**Nystatin µg/mL**	
Fungal isolate	MIC	MFC
C. albicans	1	2
C. tropicalis	1	2
A. niger	0.5	1
A. flavus	2	4

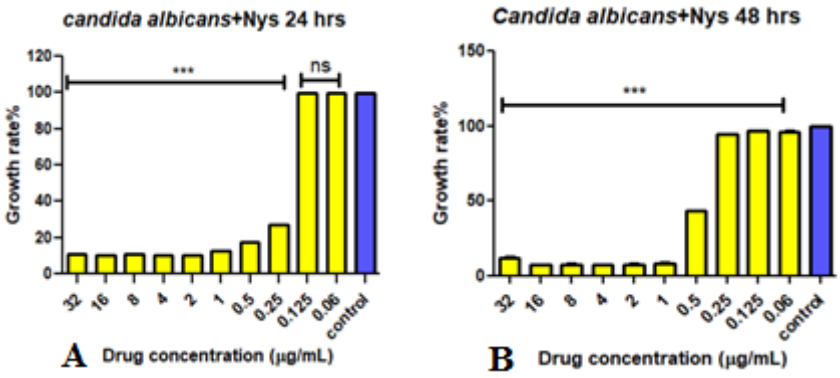

Figure 7. Represent effect of Nystatin in growth rate of *Candida albicans* A=after 24 and B=after 48 hrs. Results are displayed as a mean of 3 replicates. ns=no significant difference $p \geq 0.05$, *** $p < 0.0001$, significant difference between Nystatin and the positive control (100%).

The yeast *C. albicans* showed very low growth rates in different concentrations of Nystatin after (24 and 48) hrs. (except the concentrations (0.125 and 0.06) µg/mL, where it gave its lowest growth rate (> 10%) at concentrations (1-32) µg/mL. There is a significant difference when compared with control, see Fifure 7.

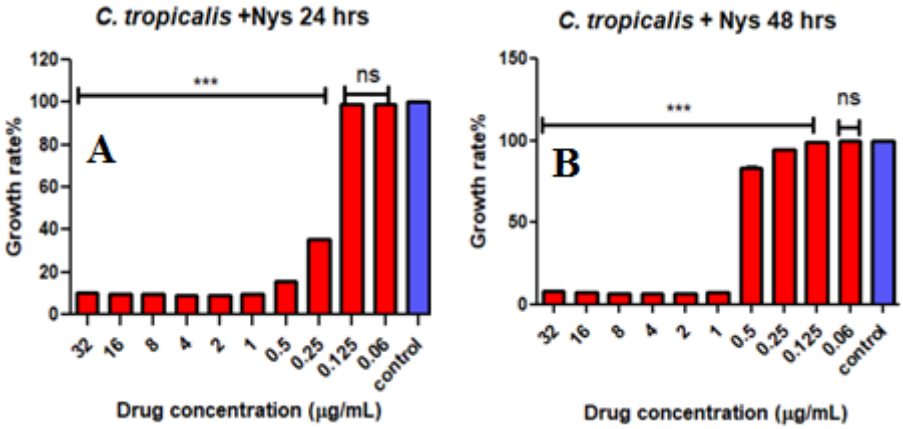

Figure 8. Represent effect of Nystatin in growth rate of *Candida tropicalis* A=after 24 and B=after 48 hrs. Results are displayed as a mean of 3 replicates. ns=no significant difference $p \geq 0.05$, *** $p < 0.0001$, significant difference between Nystatin and the positive control (100%).

Also, the yeast *C. tropicalis* showed very low growth rates after (24 and 48) h. except the low concentrations of Nystatin and also gave its lowest growth rates (> 10%) at concentrations (1-32) µg/mL. There is a significant difference when compared with control, see Figure 8.

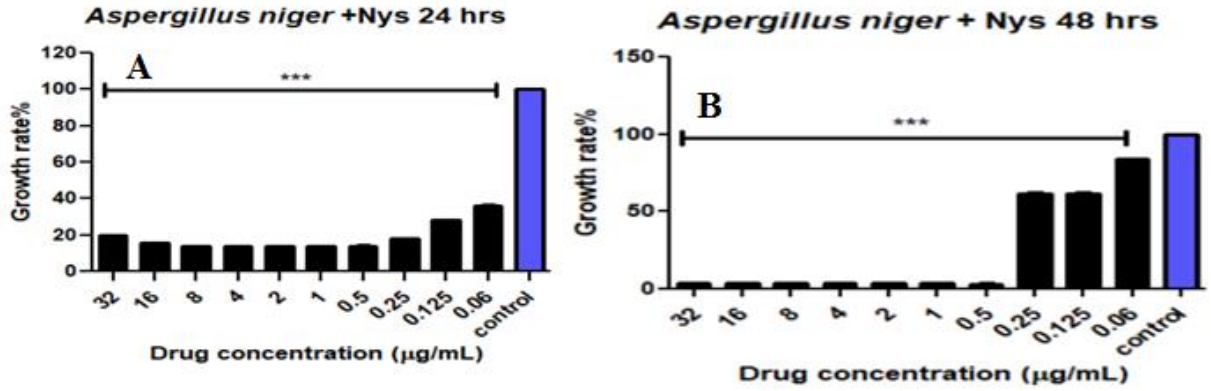

Figure 9. Represent effect of Nystatin in growth rate of *Aspergillus niger* A=after 24 and B=after 48 hrs. Results are displayed as a mean of 3 replicates. ns=no significant difference $p \geq 0.05$, *** $p < 0.0001$, significant difference between Nystatin and the positive control (100%).

The filamentous fungus *A. niger* showed a great response to different concentrations of Nystatin, and after 48 hrs. gave a very low growth rate (> 5%) in the concentrations (0.5-32) µg/mL and a significant difference when compared with control, see Figure 9.

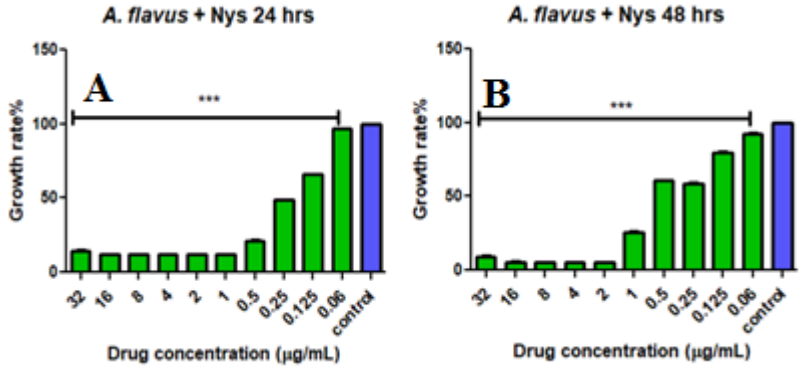

Figure 10. Represent effect of Nystatin in growth rate of *Aspergillus flavus* A=after 24 and B=after 48 hrs. Results are displayed as a mean of 3 replicates. ns=no significant difference $p \geq 0.05$, *** $p < 0.0001$, significant difference between Nystatin and the positive control (100%).

The Figure 10 shows the growth rates of *A. flavus* at different concentrations of Nystatin, where their growth rates were low at concentrations (0.5- 32) µg/mL and afforded a significant difference when compared with the control. The effect of Au NPs on the studied pathogenic fungi was tested, see Figure 11, and they compared with positive control (pathogenic fungi alone).

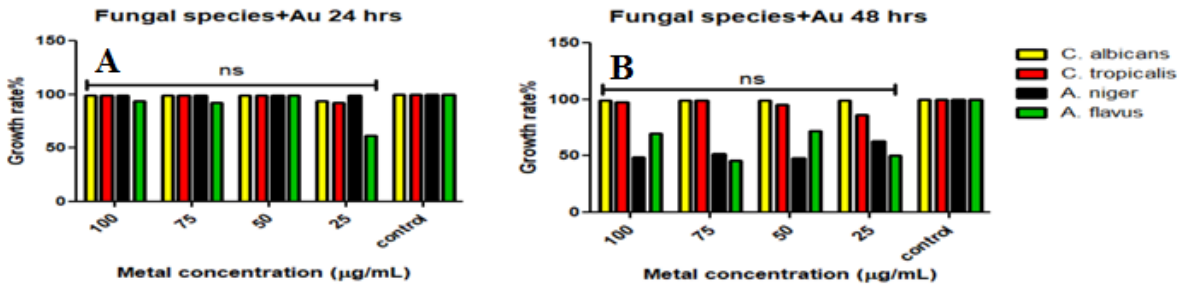

Figure 11. Represent effect of Au NPs in growth rate of pathogenic fungi A=after 24 and B=after 48 hrs. Results are displayed as a mean of 3 replicates. ns=no significant difference $p \geq 0.05$, *** $p < 0.0001$, significant difference between Au NPs and the positive control (100%).

The tested pathogenic fungi showed varying growth rates after 24 h, where the lowest growth rate was for *A. flavus* (61.5%) in the concentration (25 µg/mL). After 48 h the growth rates of *A. niger* and *A. flavus* were affected by Au NPs in the concentrations (50 and 75) µg/mL, while the growth rates of pathogenic yeasts were not affected and remained close to the control. No significant difference was shown after (24 and 48) h.

The effect of Au NPs with Nystatin on the studied pathogenic fungi was tested, see Figure 12, and they compared with positive control (pathogenic fungi alone). A combination of Nystatin with Au NPs was used to study their effect on the growth rates of pathogenic fungi (Fig. 12). Their growth rates after 24 h were low, especially the filamentous isolates, which gave a growth rate less than 25%. After 48 h, all isolates gave very low growth rates and in all concentrations. The Figure 12 showed a significant difference after (24 and 48) h.

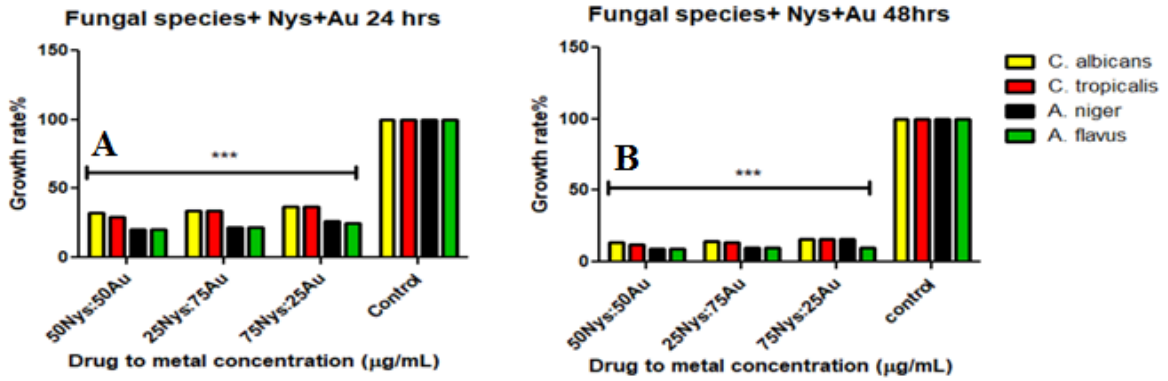

Figure 12. Represent effect of (Au NPs and Nystatin) in growth rate of pathogenic fungi A=after 24 and B=after 48 h. Results are displayed as a mean of 3 replicates. ns=no significant difference $p \geq 0.05$, *** $p < 0.0001$, significant difference between (Au NPs+ Nys) and the positive control (100%).

Cytotoxicity study of Au NPs

The cytotoxicity effect of nystatin on Vero cell line is shown in (Fig. 13) After 48h. incubation the high concentrations of nystatin were significantly affect in cells comparing

to control as shown in Figure 13, while the nystatin range of concentrations from 8-1µg/mL were no toxic. These concentrations had high viability cells which reached above 88% at 1µg/mL as displayed in Figure 13.

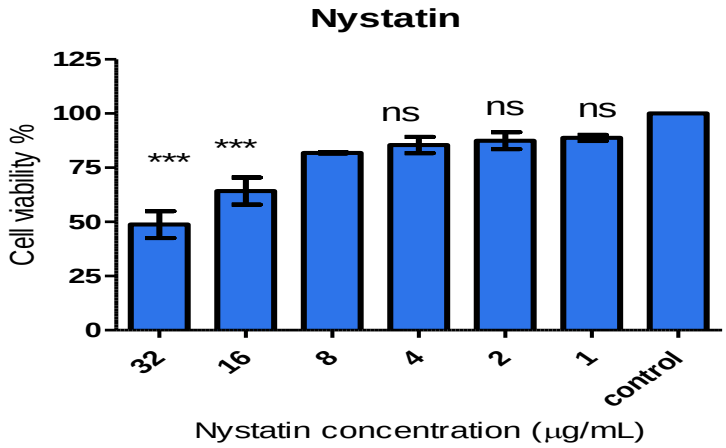

Figure 13. Percentage viability of Vero cells monolayer cells after 48 h. exposure to various concentrations of nystatin utilising MTT assay. Results are displayed as a mean of 3 replicates. ns=no significant difference $p \geq 0.05$, *** $p < 0.001$, significant difference between Nystatin and the negative control (100%).

The toxic effect of gold nanoparticles on Vero cells illustrated in (Fig. 14). The 25% concentration was non-toxic on cell viability while other concentrations (50%, 75%) v/v showed significant negative effect on cell viability Figure 14.

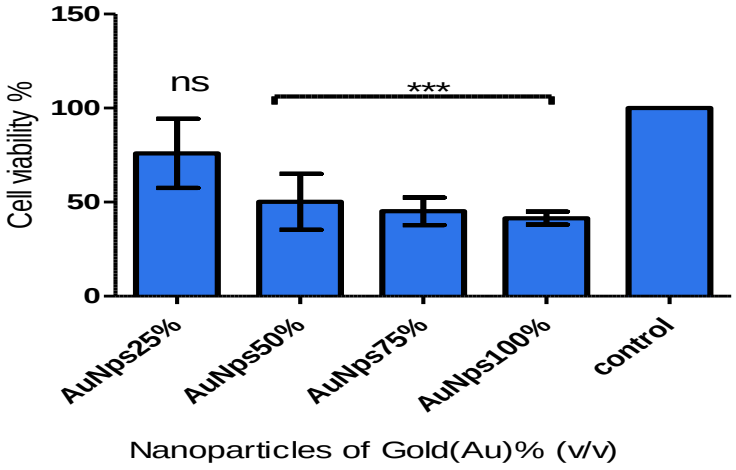

Figure 14. Percentage viability of Vero cells monolayer cells after 48 h. exposure to various concentrations of selenium nanoparticles utilising MTT assay. Results are displayed as a mean of 3 replicates. ns=no significant difference $p \geq 0.05$, *** $p < 0.001$, significant difference between Au NPs and the negative control (100%).

The cytotoxic profile of nystatin with Au NPs is highlighted in (Fig. 15), all concentrations of Au NPs were toxic on Vero cells, the cell viability was less than 50%

comparing to control. The statistical analysis revealed this significant effect as shown in Figure 15.

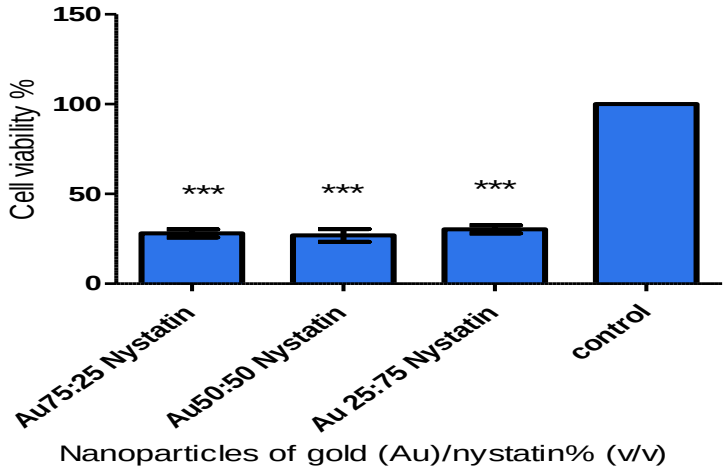

Figure 15. Percentage viability of Vero cells monolayer cells after 48h. exposure to various concentrations of nystatin and gold utilising MTT assay. Results are displayed as a mean of 3 replicates. ns=no significant difference $p \geq 0.05$, *** $p < 0.001$, significant difference between (Au NPs+ Nys) and the negative control (100%).

***In silico* study**

Protein-Ligand Binding Affinities and Docking Conformations Molecular docking simulations of Nystatin complexed with gold (Au) were performed against the target proteins 5FRB (*Aspergillus* thioredoxin reductase) and 5V5Z (metalloprotein). The results, summarized in Table 2, revealed distinct binding affinities and conformational stabilities for each metal-protein combination. For 5FRB, the Nystatin-Au demonstrated moderate affinity (-3.25 ± 0.12 kcal/mol) and stability (RMSD:28.45 ± 1.1 Å), engaging residues SER289, LEU293, and HIS296, see Table 2.

Table 2. Docking Results for Nystatin-Au NPs

Ligand-Metal Complex	Protein	Binding Energy (kcal/mol)	Docking RMSD (Å)	Key Binding Sites
Nystatin + Au	5FRB	-3.25 ± 0.12	28.45 ± 1.1	SER289, LEU293, HIS296

Protein-Ligand Interaction Profiles

Interaction analysis using PLIP (Protein-Ligand Interaction Profiler) highlighted the dominance of non-polar forces across all complexes (Table 3). For 5FRB, Nystatin-Au formed van der Waals contacts with ASP493 (3.49 Å) and TYR500 (3.67 Å), see Table 3. Notably, no hydrogen bonds were detected in complex, underscoring the critical role of van der Waals and hydrophobic forces in stabilizing metal coordination.

Table 3. Interaction Analysis.

Complex	Protein	Interaction Type	Key Residues (Distance Range)	Interaction Energy (kcal/mol)
Nystatin + Au (5FRB)	5FRB	Van der Waals	LEU293 (4.12 Å), HIS296 (4.45 Å)	-0.15 to -0.07

Role of Binding Residues and Ligand Interaction Mechanisms

The binding residues identified in 5FRB and 5V5Z play critical roles in the structural and functional integrity of these proteins. For 5FRB, a thioredoxin reductase essential for redox homeostasis, the catalytic triad ASP493, THR498, and TYR500 facilitates electron transfer during the reduction of thioredoxin.

Domain-Specific Effects of Ligand Binding

The Nystatin-Au interacted with SER289 and HIS296, inducing conformational changes that destabilized NADPH binding. This allosteric modulation disrupted the enzyme's ability to utilize NADPH as an electron donor, compromising redox homeostasis and amplifying oxidative stress.

Molecular Dynamics (MD) Simulations

Fifty-nanosecond MD simulations validated the stability and flexibility of Nystatin-Au NPs, see Table 4 and Figure 16. The Nystatin-Au-5FRB NPs exhibited the lowest structural deviation (RMSD: 1.98 ± 0.2 Å) and persistent hydrogen bonding (5 ± 1 bonds), indicating robust stability.

Table 4. MD Simulation Metrics.

Complex	Avg. RMSD (Å)	Avg. RMSF (Å)	Hydrogen Bonds	SASA (Å²)
Nystatin + Au (5FRB)	1.98 ± 0.2	1.45 ± 0.1	5 ± 1	38.12

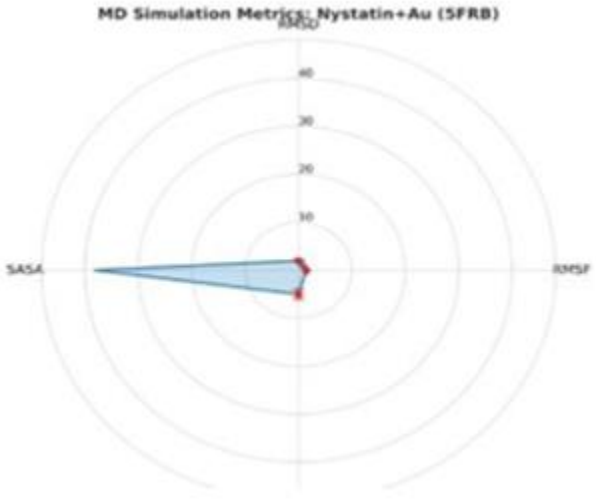

Figure 16. Molecular Dynamics Simulation Analysis of Nystatin-Au NPs.

The Nystatin-Au-5FRB complex demonstrates the highest structural stability, as evidenced by its lowest RMSD value (1.98 Å) and persistent hydrogen bonding network (5 bonds), which correlates with its robust stability in your binding studies. The solvent-accessible surface area (SASA) analysis reveals an important trend.

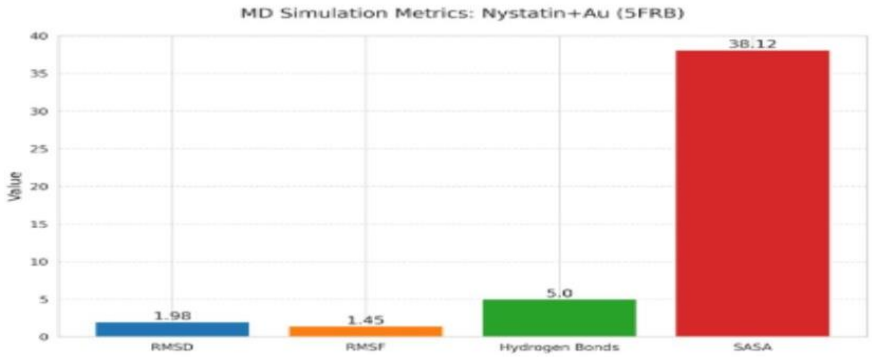

Figure 17. presents a comparative visualization of these stability metrics through bar graphs.

The panel (Nystatin-Au-5FRB) underscores its exceptional stability, with the lowest RMSD (1.98 Å) and highest hydrogen bond count (5.0), aligning with your data on catalytic site retention. These figures validate the inverse correlation between SASA and flexibility observed in your analysis, while demonstrating how hydrogen bonding and metal coordination geometry collectively govern complex stability.

Toxicity study *in silico* using Pro Tox 3.0 software

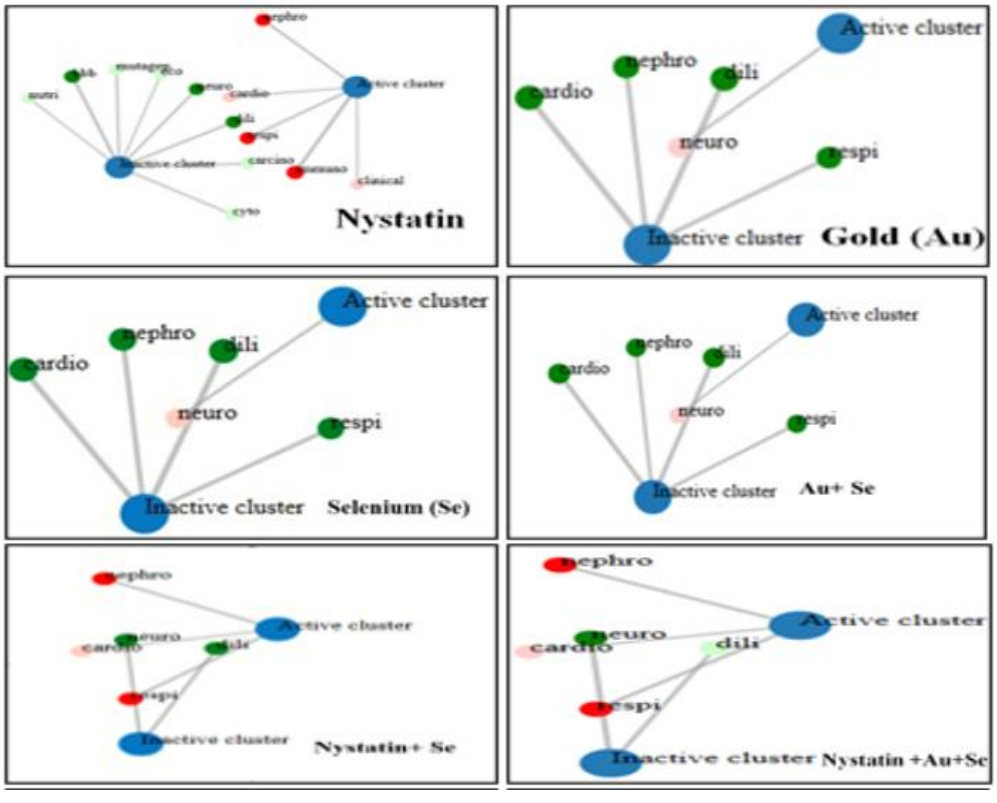

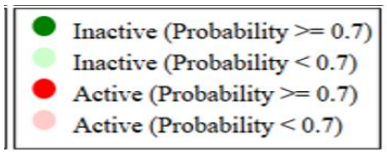

Figure 18. *In silico* study using Pro Tox 3.0 software to detect the toxicity of Au NP.

Recently, using in silico studies give deep knowledge about toxicity drug and materials, particularly that deals with organ like Pro Tox 3.0. This program explains the details about organ toxicity and toxicity end point. Current data that obtained by this program showed the toxicity of Au NPs as well as Nystatin that used as antifungal standard, see Figure 18.

The most organs that affected were nephro and respiratory systems. Gold NPs were not toxic to tested organs. The combination of Au NPs with Nystatin showed toxicity in nephro and respiratory systems. Similar effect has showed for Nystatin (Fig. 18).

Discussion

Au NPs possess unique qualities such as adjustable size, shape, surface properties, optical properties, biocompatibility, low cytotoxicity and high stability that make them important in many medical applications. Au NPs are characterized by their activity against bacteria and fungi, where antimicrobial drugs can bind with Au NPs through covalent or non- covalent bonds using NPs as carrier of antimicrobial drugs, which increases the effectiveness of reaching them to the target [32]. The biosynthesis method gave good results within three days, the colour of the mixture of biomass was changed. But after that the NPs withdrawn inside the fungal biomass, so that the colour of nanofluid became transparent. The colour of fungal biomass changed to the colour of nanofluid, this behaviour may be due to high concentration of NPs which lead to high toxicity in the solution, so the fungus pulls the NPs out of the solution to reduce its toxicity.

Metal NPs was characterized by different methods, these methods helped in confirm the existence of NPs. UV-Vis spectrometry is the first method was used to characterized the existence of NPs. The Au NPs gave their maximum absorption peak at a wavelength 540 nm. The (FTIR) method is a type of spectroscopy that can reveal changes in the overall composition of biomolecules by identifying changes in functional groups. TEM is a powerful tool for studying shape and size of NPs, green synthesis of NPs inside the microorganism required to showing the microbial effect in physical characterization due to microbial enzyme that use mainly to produce these NPs. In recent study, fungal enzymes from different fungi (*T. asperellum, P. camemberti, A. cejpii)* involve in NPs production, leading to produce certain physical features like size and shape depending on the type of enzymes. The TEM results of *T. asperellum* revealed the AuNPs inside the fungal cell. According to the pictures the shape of AuNPs spherical and abundant inside the fungal cell.

The studied pathogenic fungi showed a significant effect in different concentrations of Nystatin alone, as their growth rates gave a significant difference. When the Nystatin was mixed with Au NPs for increased synergistic antimicrobial potential against pathogenic fungi the growth rates gave a clear significant difference.

Antimicrobial resistance poses a serious and growing threat to society however, the emergence of fungi resistant to multiple treatments has led to an urgent need for new, effective and safe antifungal agents [33]. *In vitro* cytotoxicity tests are an important step through the drug designing and development its derivatives. In general, using cell lines in evaluating drug toxicity is not sophisticated and relatively. In recent study, the nano-toxic activity of green synthesized Au NPs and nystatin were tested *in vitro* using Vero cell line by applying MTT assay. Results of this metabolic-based test were summarized in Figures (7-10). Using Vero cells line for nystatin, toxic profile was safe at concentrations ranged from 8-1 μg/mL). This result similar to what the previously found by Tevyashova *et al.* [34]. However, the combination of nystatin with Au NPs was not encouraged due to obvious toxic effect in tested cells. Several factors cause nanotoxicity to Au NPs like size, shape, surface charge, and surface chemistry [35].

Nystatin toxicity was established in skin and kidney *in vivo*. Improvement of antifungal drugs using NPs such as Au have been studied. Prediction of toxicity for NPs and drugs have been controversial issue because these studies depend on dose of drug or NPs properties. Computational model are promising tools to predict toxicity using different parameters and give a precious insight about profile toxicity; however, these programs require experimental validations.

CONCLUSION

Fundamental Finding : Green synthesis NPs using filamentous fungi is a promising approach, due to the perfect enzyme system that makes them a powerful tool to produce nanoparticles efficiently and economically. This highlights the unique biochemical potential of filamentous fungi in nanotechnology, providing a sustainable alternative to conventional synthetic methods. **Implication :** The utilization of filamentous fungi for nanoparticle synthesis not only offers cost-effective and eco-friendly benefits but also aligns with the growing demand for green chemistry solutions in biomedical and industrial applications. Their enzymatic versatility opens new avenues for scalable and targeted nanoparticle production. **Limitation :** However, despite its promise, this method still faces challenges in achieving consistent control over nanoparticle characteristics. Additionally, current computerized prediction tools used in designing such systems lack comprehensive experimental validation, limiting their precision in accounting for diverse biological parameters. **Future Research :** Future optimization should focus on hydrophobic moiety engineering, as suggested by structure-based drug design principles. Computerized prediction tools need more experimental validation to cover more biological parameters to increase their accuracy, which will be critical in enhancing the reliability and applicability of fungal-mediated nanoparticle synthesis.

ACKNOWLEDGMENTS

We would like to thank Dr. Nawras T. Jassim and Dr. Israa M. Shamkh for conducting the *in silico* study.

REFERENCES

[1] D. Suhag, P. Thakur, and A. Thakur, "Introduction to Nanotechnology," *Integrated Nanomaterials and their Applications*, *Singapore: Springer Nature Singapore*, pp. 1–17, 2023.

[2] R. Sharma, K. S. Sharma, and D. Kumar, "Introduction to Nanotechnology," *Nanomaterials in Clinical Therapeutics: Synthesis and Applications*, *Singapore: Springer Nature Singapore*, pp. 1–31, 2022.

[3] A. Haleem, M. Javaid, R. P. Singh, S. Rab, and R. Suman, "Applications of Nanotechnology in Medical field," *Global Health Journal*, vol. 7, no. 2, pp. 70–77, 2023.

[4] Y. Khan *et al.*, "Classification, Synthetic, and Characterization Approaches to Nanoparticles, and Their Applications in Various Fields of Nanotechnology: A Review," *Catalysts*, vol. 12, no. 11, pp. 1386, 2022.

[5] J. M. Domingues, C. S. Miranda, N. C. Homem, H. P. Felgueiras, and J. C. Antunes, "Nanoparticle Synthesis and Their Integration into Polymer-Based Fibers for Biomedical Applications," *Biomedicines*, vol. 11, no. 7, pp. 1862, 2023.

[6] S. Khan and M. K. Hossain, "Classification and properties of nanoparticles," *Nanoparticle-Based Polymer Composites*, pp. 15–54, 2022.

[7] N. Joudeh and D. Linke, "Nanoparticle classification, physicochemical properties, characterization, and applications: a comprehensive review for biologists," *Journal of Nanobiotechnology*, vol. 20, no. 1, 2022.

[8] D. Qiao, T. Zhang, and M. Tang, "Autophagy regulation by inorganic, organic, and organic/inorganic hybrid nanoparticles: Organelle damage, regulation factors, and potential pathways," *Journal of Biochemical and Molecular Toxicology*, vol. 37, no. 10, 2023.

[9] K. Hachem *et al.*, "Methods of Chemical Synthesis in the Synthesis of Nanomaterial and Nanoparticles by the Chemical Deposition Method: A Review," *BioNanoScience*, vol. 12, no. 3, pp. 1032–1057, 2022.

[10] I. A. Jaffer Al-Timimi, P. A. Sermon, A. A. Burghal, A. A. Salih, and I. M. N. Alrubaya, "Nanoengineering the antibacterial activity of biosynthesized nanoparticles of TiO_2, Ag, and Au and their nanohybrids with Portobello mushroom spore (PMS) (TiO_x/PMS, Ag/PMS and Au/PMS) and making them optically self-indicating," *SPIE Proceedings*, vol. 9930, pp. 99300B, 2016.

[11] A. Taheriazam *et al.*, "Eco-friendly chitosan-based nanostructures in diabetes mellitus therapy: Promising bioplatforms with versatile therapeutic perspectives," *Environmental Research*, vol. 228, pp. 115912–115912, 2023.

[12] H. S. Devi, M. A. Boda, M. A. Shah, S. Parveen, and A. H. Wani, "Green synthesis of iron oxide nanoparticles using Platanus orientalis leaf extract for antifungal activity," *Green Processing and Synthesis*, vol. 8, no. 1, pp. 38–45, 2019.

[13] B. T. Sone, A. Diallo, Xolile Fuku, A. Gurib-Fakim, and M. Maaza, "Biosynthesized CuO nano-platelets: Physical properties & enhanced thermal conductivity nanofluidics," *Arabian Journal of Chemistry*, vol. 13, no. 1, pp. 160–170, 2020.

[14] T. Singh, N. Srivastava, P. K. Mishra, and A. K. Bhatiya, "Analysis of Various Green

Methods to Synthesize Nanomaterials: An Eco-Friendly Approach," *Clean Energy Production Technologies*, pp. 181–205, 2021.

[15] A.-T. Iman, "Metal and oxide nanoparticles: Green biosynthesis using Portobello Mushroom Spores (PMS) for nanocomposites and replicas, properties and applications," *Brunel.ac.uk*, 2018.

[16] K. Umamaheswari and M. Abirami, "Assessment of antifungal action mechanism of green synthesized gold nanoparticles (AuNPs) using Allium sativum on Candida species," *Materials Letters*, vol. 333, pp. 133616, 2023.

[17] S. I. Manzoor *et al.*, "Green synthesis of biocompatible silver nanoparticles using *Trillium govanianum* rhizome extract: comprehensive biological evaluation and *in silico* analysis," *Materials Advances*, vol. 6, no. 2, pp. 682–702, 2024.

[18] A. A. Alkhafaji *et al.*, "Pharmaceutical properties for green fabricated ZnO and Ag nanoparticle-mediated *Borago officinalis*: *In silico* predications study," *Green Processing and Synthesis*, vol. 14, no. 1, 2025.

[19] T. A. Halgren, "Identifying and Characterizing Binding Sites and Assessing Druggability," *Journal of Chemical Information and Modeling*, vol. 49, no. 2, pp. 377–389, 2009.

[20] G. Madhavi Sastry, M. Adzhigirey, T. Day, R. Annabhimoju, and W. Sherman, "Protein and ligand preparation: parameters, protocols, and influence on virtual screening enrichments," *Journal of Computer-Aided Molecular Design*, vol. 27, no. 3, pp. 221–234, 2013.

[21] A. Messaoudi, H. Belguith, and J. Ben Hamida, "Homology modeling and virtual screening approaches to identify potent inhibitors of VEB-1 β-lactamase," *Theoretical Biology and Medical Modelling*, vol. 10, no. 1, pp. 1–10, 2013.

[22] P. VASANTHI BATHRINARAYANAN, D. THANGAVELU, V. K. MUTHUKUMARASAMY, C. MUNUSAMY, and B. GURUNATHAN, "Biological synthesis and characterization of intracellular gold nanoparticles using biomass of Aspergillus fumigatus," *Bulletin of Materials Science*, vol. 36, no. 7, pp. 1201–1205, 2013.

[23] CLSI, "Performance Standards for Antimicrobial Susceptibility Testing," 15th Informational Supplement, M100-S15, *Clinical and Laboratory Standards Institute*, Wayne, 2008.

[24] Y. M. Mohamed, A. M. Azzam, B. H. Amin, and N. A. Safwat, "Mycosynthesis of iron nanoparticles by Alternaria alternata and its antibacterial activity," *African Journal of Biotechnology*, vol. 14, no. 14, pp. 1234–1241, 2015.

[25] H. M. Berman and S. K. Burley, "Protein Data Bank (PDB): Fifty-three Years Young and Having a Transformative Impact on Science and Society," *Quarterly Reviews of Biophysics*, vol. 58, pp. 1–50, 2025.

[26] G. M. Morris *et al.*, "AutoDock4 and AutoDockTools4: Automated docking with selective receptor flexibility," *Journal of Computational Chemistry*, vol. 30, no. 16, pp. 2785–2791, 2009.

[27] S. Kim and E. E. Bolton, "PubChem: A Large-Scale Public Chemical Database for Drug Discovery," *Methods and principles in medicinal chemistry*, pp. 39–66, 2023.

[28] Mohammed *et al.*, "Green Synthesis of Zinc Oxide Nanoparticles Using *Cymbopogon citratus* Extract and Its Antibacterial Activity," *ACS Omega*, vol. 8, no. 35, pp. 32027–32042, 2023.

[29] M. F. Adasme *et al.*, "PLIP 2021: expanding the scope of the protein–ligand interaction profiler to DNA and RNA," *Nucleic acids research*, vol. 49, no. 1, pp. 530-534, 2021.

[30] S. Iranmanesh, G. H. Shahidi Bonjar, and A. Baghizadeh, "Study of the biosynthesis of gold nanoparticles by using several saprophytic fungi," *SN Applied Sciences*, vol. 2, no. 11, 2020.

[31] B. Zimmermann, Z. Tkalčec, A. Mešić, and A. Kohler, "Characterizing Aeroallergens by

Infrared Spectroscopy of Fungal Spores and Pollen," *PLOS ONE*, vol. 10, no. 4, pp. e0124240, 2015.

[32] C. Su, K. Huang, H.-H. Li, Y.-G. Lu, and D.-L. Zheng, "Antibacterial Properties of Functionalized Gold Nanoparticles and Their Application in Oral Biology," *Journal of Nanomaterials*, vol. 2020, no. 1, pp. e5616379, 2020.

[33] J. Ito, Kriengkauykiat, S. Dadwal, and Kriengkauykiat, "Epidemiology and treatment approaches in management of invasive fungal infections," *Clinical Epidemiology*, vol. 3, pp. 175, 2011.

[34] A. Tevyashova *et al.*, "Semisynthetic Amides of Amphotericin B and Nystatin A1: A Comparative Study of In Vitro Activity/Toxicity Ratio in Relation to Selectivity to Ergosterol Membranes," *Antibiotics*, vol. 12, no. 1, pp. 151, 2023.

[35] A. M. Alkilany, N. N. Mahmoud, F. Hashemi, M. J. Hajipour, F. Farvadi, and M. Mahmoudi, "Misinterpretation in Nanotoxicology: A Personal Perspective," *Chemical Research in Toxicology*, vol. 29, no. 6, pp. 943–948, 2016.

***Suaded A. Majeed (Correspondence)**
University of Basrah, Iraq
Email: mustafafadil837@gmail.com

Iman A. J. Al-Timimi
University of Basrah, Iraq

Abdullah H. Al-Saadoon
University of Basrah, Iraq